SSRG International Journal of Electrical and Electronics Engineering
ISSN: 2348-8379/ https://doi.org/10.14445/23488379/IJEEE-V13I7P107

Volume 13 Issue 7, 125-144, July 2026

Original Article

Design Optimization and Operating Performance Comparative Evaluation of a Five-Phase Fault-Tolerant Spoke-Type Interior Permanent Magnet and Stator Permanent Magnet Flux-Switching Motors for Electric Vehicle Traction Application

Godwin Eshun[1], Stephen Eduku[2*]

[1,2]*Department of Electrical and Electronic Engineering, Faculty of Engineering, Takoradi Technical University, Takoradi, Ghana.*
[2]*Department of Nautical Studies, Faculty of Maritime and Nautical Studies, Takoradi Technical University, Takoradi, Ghana.*

[*]*Corresponding Author : 5103180335@stmail.ujs.edu.cn*

Received: 04 September 2025 Revised: 03 June 2026 Accepted: 23 June 2026 Published: 27 July 2026

Abstract - *The five-phase Stator Permanent Magnet Flux-Switching (Stator PMFS) motor and Five-Phase Spoke-Type Interior Permanent Magnet (Spoke-Type IPM) motor have been recently utilized extensively in Electric Vehicle (EV) traction applications due to their fault-tolerant nature in the event of a fault compared to their three-phase design counterparts. Nonetheless, these two motors, with the same design parameters and specifications, have not been designed, optimized, and compared simultaneously for EV traction applications, thereby creating a gap in the literature. Hence, this research work aimed at comparing the five-phase Stator PMFS motor and Spoke-Type IPM motor with the same design parameters and specifications via the Finite Element Analysis (FEA) through the Ansys Maxwell electromagnetic software to unearth the preferred candidate for EV traction applications based on electromagnetic torque, operating efficiency, minimal torque ripple, and power and torque densities. Furthermore, the adopted multi-objective optimization is a synergy between the Surface Response Method (RSM) and Bare-Bones Multi-Objective Particle Swarm Optimization (BB_MOPSO). Moreover, the Spoke-Type IPM motor exhibits an 18.4% increase in electromagnetic torque with minimal torque ripple compared to the Stator PMFS motor. Also, the Spoke-Type IPM motor unveils an efficiency of 1.17% increase compared to the Stator PMFS motor. Meanwhile, the Spoke-Type IPM motor unveils a 17.5% increase in power density and an 18.42% increase in torque density compared to the Stator PMFS motor. Thus, the Spoke-Type IPM motor is a suitable or preferred design candidate for EV traction applications.*

Keywords - *EV Traction, Five-Phase Fault-Tolerant, FEA, Multi-Objective Optimization, Stator PMFS Motor, Spoke-Type IPM Motor.*

1. Introduction

Electrical machines, especially permanent magnet brushless AC motors, are fast emerging as the heart of the electric vehicle traction application due to global warming as a result of greenhouse emissions and environmental pollution, with predominant utilization of Internal Combustion (IC) engine vehicles, and PM motors' ability to maximize the operating efficiency owing to the absence of excitation windings. Moreover, extensive research has focused on three-phase Permanent Magnet (PM) motors compared with multiphase motor designs. Besides, it is essential to underscore that the three-phase motor comes with very minimal fault-tolerant capacity, which limits its application in such critical applications compared to the multiphase motors. Moreover, Electric Vehicles (EVs) are progressively permeating the market, offering users and operators an obvious zero-emission or pollution solution for personal mobility [1].

However, the flux-switching machine was first unveiled as a well-designed generator with a single-phase configuration in 1955, which did not gain a considerable research attention until recent time when multiphase flux-switching PM stator machine designs commenced with extensive investigation, meanwhile, the stator PM flux-switching motor exhibit many key design features, not excluding PMs arranged on the laminated stator, non-winding rotor pole making it simple and robust, sinusoidal back-emf with higher electromagnetic torque production capacity [2-11].

Moreover, permanent magnet brushless flux-switching motors are widely and extensively investigated to unveil or demonstrate the robustness of a salient rotor design due to non-magnetic and winding arrangement on the rotor core, but rather have the Permanent Magnet (PM) configured on its stator core, and an identical design candidate to its design counterpart of the switched reluctance motor, which enhances temperature management of the PMs [12].

The stator-designed PM motors have been unveiled as a novel motor configuration with the design synergy of the PM and phase armature configured windings presented in the laminated design stator structure or core, besides, these Flux-Switching PM Motors (FSPMM) have widely gain research attention owing to their flux-density and robustness rotor exhibition with easy of thermal or heat dissipating management of the PMs, moreover, multiphase motors are imperative to numerous crucial safety application in sectors, such as traction of Electric Vehicle (EV), power generation via wind source and aerospace, owing to an enhanced fault-tolerant capacity and the degree of phase freedom that minimized the power burden or stress per phase [13-17].

Moreover, to enhance an electromagnetic torque density or capacity, researchers or scholars proposed a motor topology with spoke-type designed ferrite magnets to ensure concentrated magnetic flux effect [18]. Meanwhile, it is evidenced by researchers in [19] that the utilization of the spoke-type structure in addition to hybrid magnets simultaneously unveils or exhibits relatively higher operating torque and power densities, and demonstrates its cost-effectiveness. Furthermore, interior PM motor exhibit greater design consideration than the traditional PM synchronous motor due to its unique technical design robustness, higher torque density exhibition and wider operating speed range, meanwhile, the unveil cogging torque and exhibition of harmonic content variation in the motor air gap established flux-density has obviously made the interior PM synchronous motor, being one of the key design challenges, nonetheless, spoke-type interior PM design arrangement with extensive optimization of the motor can unveil higher torque density for electric vehicle traction application[20-23].

Moreover, the interior permanent magnet motors have an inherent design feature of flux concentration in the rotor, which has been demonstrated to be an effective feature or solution to magnetic flux leakage reduction and to enhance operating efficiency [24]. Meanwhile, among Interior Permanent Magnet (IPM) design machines have gain merit of flux focusing or concentrating effect of the configured Permanent Magnets (PMs) located in the core of the rotor structure, the designed spoke-type configured PM motors can enhance the rate of PM utilization, nonetheless, the demerit of this spoke-type motor is its relatively higher airgap harmonic contents which unveil higher operating torque ripple of which many scholars or researchers have extensively investigated via optimization [25-32].

Meanwhile, a multiphase PM motor topology with configured fractional-slot phase winding exhibits an inherently higher fault-tolerant operating or running capacitance due to or in light of the increased design phase selected number compared to the conventionally designed three-phase motor with limited degrees of freedom [33]. Furthermore, the spoke-Type design motors have been extensively tested and verified in terms of their operating performance and application feasibility in EV traction [34]. Meanwhile, an extensive investigation or exploration into achieving design trade-offs of higher exhibited torque density production and higher operating design efficiency of the drive system cycle was realized in a Spoke-Type PM design motor in [35] for an Electric (E) race driving cycle. Hence, extensively comparing the Spoke-Type IPM design motor with the Stator PMFS-designed motor is a key and hot research gap to be addressed in the existing motor design literature for EV traction.

Fault-tolerant motor is extremely imperative for many distinct applications, namely, aerospace and electric vehicle drive system, moreover, researchers have in recent times or years developed some multiphase fault-tolerant motor, namely, switched reluctance and conventional PM designed brushless motor, nonetheless, the switched reluctance motor suffer from or unveil lower efficiency, while the conventional PM motor unveil mechanically week design structure, meanwhile, scholars or researchers have recently unveiled a new design class or category of brushless motor with PMs configured in the laminated stator, which is referred to as flux-switching PM motors which exhibits higher efficiency, robust mechanical design integrity and strong design immunity against thermal issues [36-41].

Meanwhile, the robust and resilient fault-tolerance capacity of electrically designed motors, such as PM motors, is of great relevance and key in motor design systems for ensuring smooth and reliable motor operation [42].

Furthermore, a multiphase-designed motor drive system, which obviously depicts an additional phase compared to its design counterpart, the three-phase design motor drive system, has gained extensive attention from a research point of view in recent times or years, owing to some intrinsic merits which it exhibits when compared and contrasted to its design counterpart or candidate, the three-phase topology [43]. Nonetheless, Polyphase (multiphase) designed machines, especially motors, have been sported as a classy design alternative to their three (3) phase design counterparts or candidates in terms of higher operating power safety-crucial design applications, in contrast to the three phase machine designs, polyphase machines unveil a minimal current rating per phase since the generated power flow is split or divided amongst a high number of machine phase with an intrinsic fault-tolerant operating capacity [44-46].

Moreover, a flux-switching-designed Permanent Magnet Motor (PMM) and the Interior Permanent Magnet-Designed Motor (IPM) utilized in the 2004 Prius-designed HEV were compared extensively in [47], via a quantitative approach to unveil the preferred candidate motor design for distinct electrified transportation, namely, EVs and HEVs, not excluding the Plug-In Evs (PHEVs).

To ensure clarity and avoid misleading researchers and scholars, it is of great imperative or importance to highlight that the proposed research considered in this paper is to systematically design, model, optimized, and extensively compare the Stator PMFS motor and Spoke-Type IMP motor with the same design parameters and specification to ensure fair design comparison to scientifically established which of these aforementioned two distinct motors is suitable for EV traction application.

Meanwhile, the Stator PMFS motors and Spoke-Type IPM motors designs have been widely utilized in EV traction applications, but have not been designed, modelled, optimized, and compared with the same design parameters and design specifications to enable scholars and researchers to ascertain, based on a fair comparison, which of these two motor topologies is the suitable candidate for EV traction applications. Hence, making it a key, relevant, and current research gap that needs to be addressed by emerging research in the field of motor design.

Hence, from the aforementioned extensive review and analysis of existing literature of Stator PMFS and Spoke-Type IPM motors, it is imperative to design, optimize, analyze, and compare the five-phase fault-tolerant Stator PMFS motor and the five-phase fault-tolerant design Spoke-Type IPM motor with the same design parameters and design specifications for EV traction applications to not only address the identified research niche or gap but also as an innovative contribution to the scientific research community of motor design and research field.

Besides, the evaluation of these two motors is based on electromagnetic torque, torque ripple, power density, torque density, and operating efficiency, which are key to ensuring smooth operation in EV traction applications.

The novelty contribution of the proposed research is the designing, modelling, optimizing, analyzing, and evaluating the effective operating performance of the five-phase configured fault-tolerant Stator PMFS motor and five-phase configured fault-tolerant Spoke-Type IPM motor with the same design parameters and design specifications to ensure fair design comparison which is the identified and relevant current research gap in the existing literature to unveil the potential or suitable motor topology among the two aforementioned motors considered in this research paper for EV traction application in terms of key requirements of EV traction, such as higher electromagnetic torque, torque density, fault-tolerant capacity, and power density, operating efficiency, and minimal torque ripple and cogging torque.

2. Materials and Methods

2.1. Motor Topology Design Analysis

This section describes in detail the analysis and illustration of the two distinct five-phase design fault-tolerant Permanent Magnet (PM) motor topologies, namely, the Stator Permanent Magnet Flux-Switching Motor (Stator PMFS motor) and Spoke-Type Interior Permanent Magnet Motor (Spoke-Type IPM motor).

Moreover, the Stator PMFS motor has its PMs configured in its laminated stator core, while the Spoke-Type IPM has its PMs arranged in its laminated rotor core. Besides, the Finite Element Method (FEA) was employed or utilized to design the aforementioned two distinct motors via the ANSYS electromagnetic software.

Furthermore, the FEM is adopted for the modelling of the aforementioned motors in this paper because, among the distinct design or modelling methods, namely, the analytical method and numerical method, the Finite Element Method (FEM) is the primary or most rigorous and precise design method or technique, which is extensively and widely utilized in modelling and design of electrical machines, especially electric motor design [48].

Moreover, under this modelling technique, 2D and 3D are mostly considered, but 2D is considered in this paper, as it is widely used in motor design to reduce simulation time and ensure less design computational resources while ensuring cost-effectiveness of the design, compared to 3D, with higher computational time and much longer design simulation time.

Meanwhile, the multiphase five-phase fault-tolerant motor, namely the Stator PMFS motor and Spoke-Type motor, is designed with the same magnetic core, a laminated steel DW540 type. Besides, the permanent magnetic material employed in both motors is NdFeB35.

Moreover, the Permanent Magnets (PMs) are fixed or configured within the laminated stator core design of the Stator PMFS motor, making the rotor structure robust and improving heat dissipation. In contrast, the PMs of the designed Spoke-Type IPM motor are interiorly configured or fixed in the laminated rotor core, which enhances its air gap flux focusing capability to ensure higher torque production.

Meanwhile, the Spoke-Type IPM design motor comes with a complex rotor structure due to the rotor rib and PM arrangement compared with the Stator PMFS motor rotor topology. Furthermore, the two motors have been designed comprehensively with the same selected design parameters, materials, and dimensions to ensure fair comparison and analysis.

Nonetheless, to further ensure intuitive design analysis and comparison, the two design motors are illustrated in Figures 1(a) and (b), respectively.

Also, their design specifications are presented or tabulated in Table 1 to facilitate or buttress the design analysis.

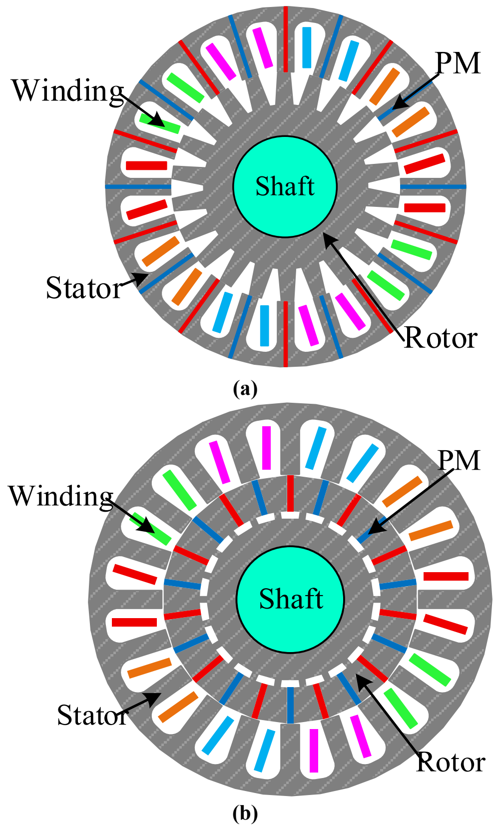

Fig. 1 Motor topologies classifications (a) Stator PMFS-Configured motor, and (b) Spoke-type IPM-Configured motor.

2.1.1. Motor Design Winding Configuration Analysis

An appropriate selection of design laminated stator and rotor pole synergy dramatically influences the production of output electromagnetic torque capability in permanent magnet design motors; hence, the design slot pole formation plays a vital role in predicting the operating output torque performance of the design motor [49, 50].

Besides, the selected rotor design pole pair, which is depicted as Pr, considered for both motor topologies, is 11, and with 20-stator slots as presented in Figure 1. Hence, unveiling that the completed adjacent established electrical angle αe between any of the two 2 configured conductor Back Electromagnetic Force (Back-EMF) is unearthed as 198 degrees, hence, establishing the precise star of slot design for the winding configuration of the motors.

Furthermore, the 198 electrical angle is obtained via the mechanical and electrical formulas presented in Equations (1) and 2, respectively. Meanwhile, the letter symbol Qs depicts the number of designed stator slots of the two motors. Moreover, the selected design stator and rotor pole synergy, which is 20-stator slots and 11-rotor pole pairs, exhibited a winding factor of 0.976, hence, an obvious prediction of higher output torque. Nonetheless, an extensive and detailed calculation and evolution of the winding star of the slot is presented in [51-53]. To ensure intuitive analysis, the winding configuration of the two motors considered in this paper is presented or demonstrated in Figures 2 (a) and (b).

$$\alpha_m = \frac{2\pi}{Q_s} = \frac{360^0}{Q_s} \tag{1}$$

$$\alpha_e = \frac{2\pi}{Q_s} p_r \tag{2}$$

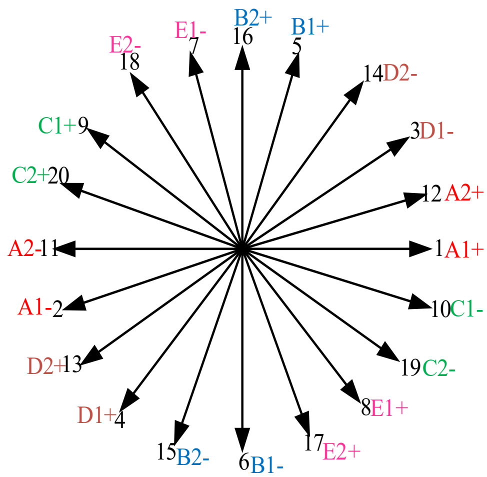

(a)

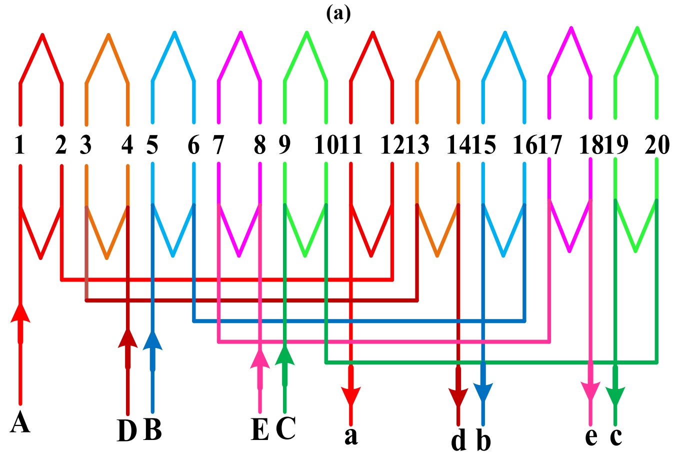

(b)

Fig. 2 Winding configuration analysis (a) Phase star of slots diagram, and (b) Winding connections.

Table 1. Design parameter specifications of the stator PMFS motor and Spoke-Type IPM configured motor

Items	Stator PMFS Motor	Spoke-Type IPM Motor
Number of stator slots/rotor poles	20/11p	20/11p
Rated motor speed (r/min)	1500	1500
Rated motor current (A)	8.2	8.2
Axial length (mm)	51.6	51.6
Stator outer diameter (SOD) (mm)	145	145
Stator inner diameter (SID) (mm)	92.7	92.7
Airgap length (mm)	0.5	0.5
Rotor outer diameter (ROD) (mm)	91.7	91.7
Rotor inner diameter (RID) (mm)	25	25
Number of turns per slot	40	40
Iron core material	DW540_50	DW540_50
PM material	N35	N35

2.1.2. Operating Principle of the Stator PMFS Motor and Spoke-Type IPM Configured Motor

To clearly elucidate the operating principle of the motor, the basic cell of the motor structure is presented in Figure 3. Moreover, the elementary (basic) cell of the motor structure contains one piece of Permanent Magnet (PM) betwixt two "U" design magnetic laminated cores, an armature phase winding, and a saliently designed rotor core. Furthermore, as illustrated in the first conjunction placement or position as presented in Figure 3 (a), the generated flux linkage produced or induced via the PM located between the two "U" stator magnetic cores is unveiled to be an arbitrary positive.

Meanwhile, in contrast, as presented in the next or second conjunction design position, as shown or demonstrated in Figure 3(b), the generated flux linkage becomes negative. Nonetheless, the operation of the Stator PMFS motor is extensively analyzed in [4, 54].

Moreover, in contrast to the Stator PMFS motor, the Spoke-Type IPM motor, as presented in Figure 4, unveils that the primary generated flux via the embedded PMs in the rotor core flows through the laminated rotor core structure, completing or establishing the magnetic loop through the motor air gap, laminated stator core, and the adjacent design stator core.

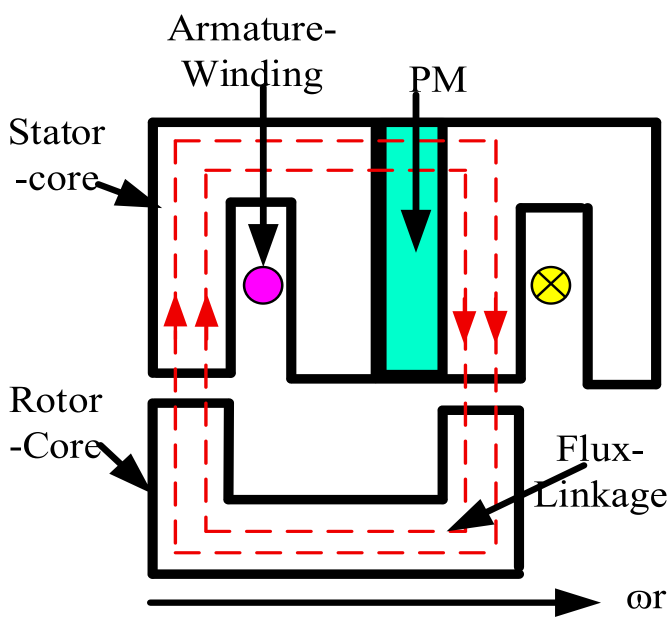

(a)

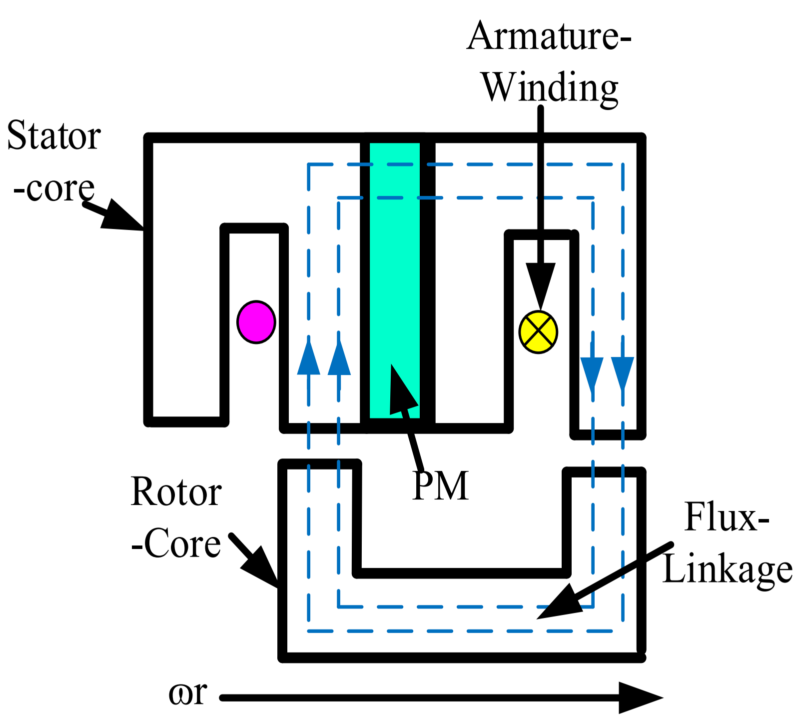

(b)

Fig. 3 Stator PMFS motor operation magnetic circuit

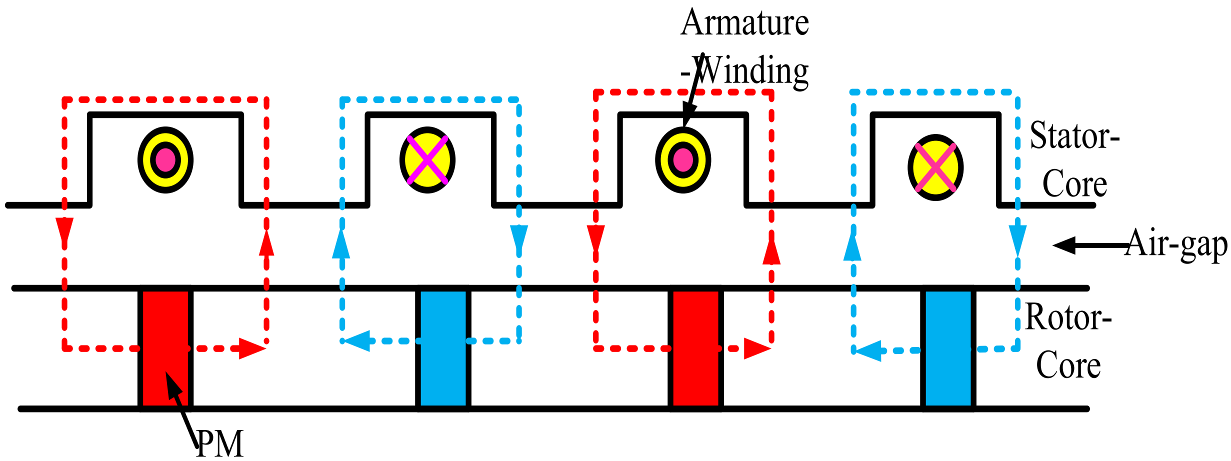

Fig. 4 Spoke-Type IPM motor operation magnetic circuit

3. Design Parameter Optimization Principle and Comparative Performance Analysis of Both Stator PMFS Motor and Spoke-Type IPM Motor

To systematically investigate distinct design strategies to enhance an electric motor's operating performance, the multi-objective motor design parameter optimization technique or method is extensively and methodologically analyzed and proven to be an effective method of optimization in [55-58] for optimizing electric motors, such as configured Permanent Magnet (PM) motors, is employed in this paper to ensure effective motor optimization. Meanwhile, Figure 5 depicts the optimized motor design parameters for the Stator PMFS motor and the Spoke-Type IPM motor. Moreover, the design parameter optimization target is to ensure minimal or infinitesimal torque ripples and enhanced output electromagnetic torque, and to ensure effective evaluation or comparative analysis of both motors considered in this paper.

Nonetheless, the optimization chronological or logical process flow diagram or chart is presented in Figure 5. To ensure fair design comparison between the Stator PMFS motor and Spoke-Type IPM configured motor, the same Permanent Magnet (PM) volume is sustained or utilized in both the Stator PMFS motor and the Spoke-Type IPM configured motor.

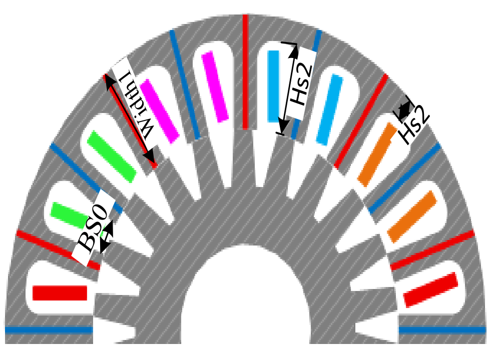

(a)

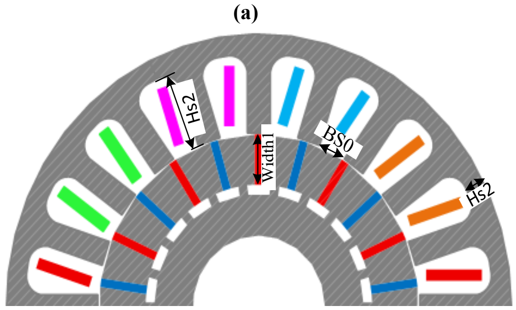

(b)

Fig. 5 Motor model for optimization (a) Stator PMFS motor, and (b) Spoke-Type IPM configured motor.

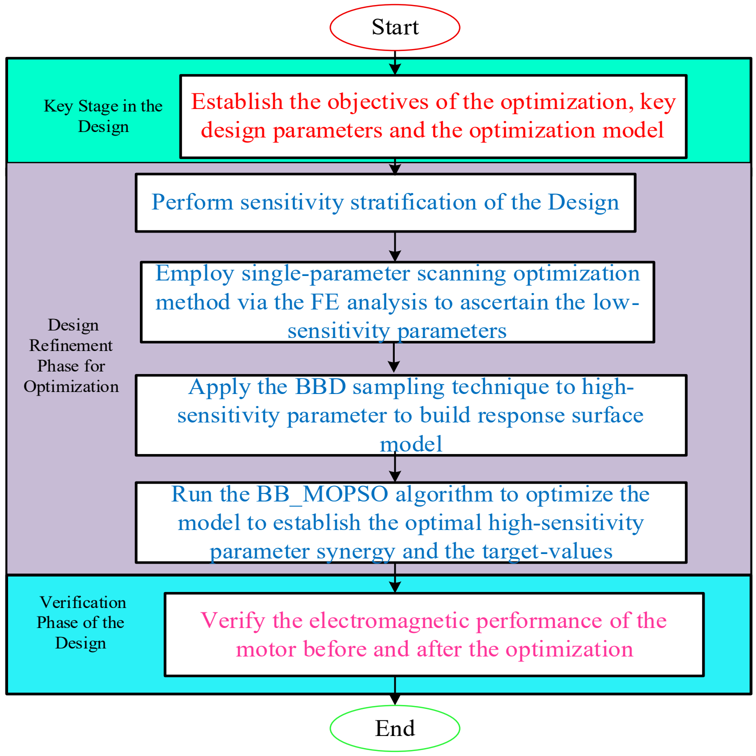

Fig. 6 Optimization logical process flow diagram of both stator PMFS motor and Spoke-Type IPM motor

3.1. Design Parameter Constraints Definition for Both Stator PMFS Motor and Spoke-Type IPM Motor Optimization Model

This research work targets the optimization of the output electromagnetic torque and a reduced operating torque ripple as key design objectives. Hence, the optimization constraints definition or conditions of both the Stator PMFS motor and the Spoke-Type IPM motor are presented in Equation (3).

$$s.t.:\begin{cases} min(x_i) \le x_i \le max(x_i) \\ g_1 = 6.8 - T_{avg} \le 0 \\ g_2 = T_{rip} - 5 \le 0 \end{cases} \tag{3}$$

Where the letter symbol Xi depicts the i^{th} term of the selected design variables, in contrast to the term T_{avg} represents the operating output average generated torque, and the term T_{rip} signifies the operating torque ripple of the aforementioned motor design topologies. Meanwhile, the initial design parameter values and their corresponding variations for both the Stator PMFS motor and the Spoke-Type IPM designed motor are presented in Tables 2 and 3, respectively.

3.1.1. Sensitivity Stratification Design Analysis of Stator PMFS Motor and Spoke-Type IPM Configured Motor

To simplify and ensure an effective optimization procedure and significantly minimize optimization time of the design, the Taguchi method or algorithm is utilized for sensitivity design analysis of the Stator PMFS motor and Spoke-Type IPM-designed motor. Nonetheless, to ensure accurate and intuitive design analysis, the model parameters of the two considered motors are presented in Figures 5(a) and (b), respectively. Furthermore, to buttress the design analysis intuitively, Tables 2 and 3 present the initial design values and associated variation ranges for each selected design parameter.

Table 2. Design parameter initial selected values and corresponding variations for stator PMFS motor

Parameter specifications	Initial Design values	Variations	Optimal Design values	FEA verification
BS0 (mm)	8.1	6.9-9.5	7	7
Width1 (mm)	12.642	10-13.62	12.612	12.612
Hs1 (mm)	2.67	2.5-2.8	2.6	2.6
Hs2 (mm)	16.4	15-17	14.65	14.65
T_{avg} (Nm)	5.41	/	6.48	6.46
T_{rip} (%)	8.26	/	4.96	3.93
$S_{pm}(mm^2)$	54.43	/	/	/

Table 3. Design parameter initial selected values and corresponding variations for Spoke-Type IPM motor

Parameter Specification	Initial Design values	Variations	Optimal Design values	FEA verification
BS0 (mm)	8.2	6.9-9.5	7	7
Width1 (mm)	11.5	10-12.86	12.84	12.84
Hs1 (mm)	2.67	2.5-2.8	2.6	2.6
Hs2 (mm)	15.4	14-17	14.4	14.4
T_{avg} (Nm)	6.11	/	7.68	7.65
T_{rip} (%)	7.38	/	4.21	3.84
$S_{pm}(mm^2)$	54.43	/	/	/

Since Permanent Magnet Volume (PMV) plays a key role in predicting electromagnetic torque output, it is very important, from a design point of view, to consistently maintain the Permanent Magnet (PM) volumes throughout the entire design optimization process.

Meanwhile, to effectively evaluate the influence or impact of each parameter of the design based on the selected or desirable design targeted objectives, namely, torque output and torque ripple, the Taguchi sensitivity technique analysis is utilized in this research work. Nonetheless, the sensitivity design values were obtained via the analysis of the mean and corresponding variance of the design selected objectives depicted via the Taguchi method tables. To buttress the intuitive analysis of the Taguchi method, Tables 4 and 5 demonstrate the design results obtained by the sensitivity analysis.

Table 4. Taguchi sensitivity design result analysis for stator PMFS motor

	Parameters	S_{com}
High design-sensitivity layer	$BS0$ (mm)	0.590783
	$width1$ (mm)	0.38657
Low design-sensitivity layer	$Hs1$ (mm)	0.001682
	$Hs2$ (mm)	0.001973

Table 5. Taguchi sensitivity design result analysis for Spoke-Type IPM motor

	Parameters	S_{com}
High design-sensitivity layer	$BS0$ (mm)	0.60783
	$width1$ (mm)	0.44748
Low design-sensitivity layer	$Hs1$ (mm)	0.001593
	$Hs2$ (mm)	0.001884

Moreover, an intuitive analysis of the optimization of both the Stator PMFS motor and Spoke-Type IPM-designed motor, the design parameters denoted as Bso and width 1, revealed a significant influence on the design objective, namely, the average torque. In contrast, the design parameters denoted with the letter symbols Hs1 and Hs2 exhibit lower design sensitivity. Furthermore, the design optimization methodology utilized in this paper is the orthogonal design tables, namely, L27L27(3^8), depicting the design code and that of the row counts corresponding to evaluating the design sensitivity of the average generated torque output and the design-obtained torque ripple relating to the PMV of the two motors. Besides, once the PMV relationship is established, the next critical analysis is the computation of the sensitivity design values for the design objective parameters. Meanwhile, the determination or establishment of the average output generated torque and the output generated torque ripple or pulsating with the aid of Finite Element Analysis (FEA) via the synergy of each design-selected parameter formulated in the design orthogonal tables. Also, the sensitivity design values are depicted as S_z for each parameter of the design, which can be unearthed via the evaluation of the mean (average) and variance of the carefully selected objective of the design, namely, the electromagnet torque and output torque ripple by employing Equation (4).

$$\begin{cases} S(z_i) = \dfrac{\theta(M(\rho|z_i))}{\theta(\rho)} \\ S_{com}(z_i) = \lambda_1 \left|S_{T_{avg}}(z_i)\right| + \lambda_2 \left|S_{Trip}(z_i)\right| \\ \lambda_1 = \lambda_2 = \dfrac{1}{2} \end{cases} \tag{4}$$

Where the letter symbol ρ represented the selected optimization design objective for the Stator PMFS motor and Spoke-Type IPM motor designs, whereas the letter symbol M ($^{\rho}/_{z}$) depicts the mean design value of the optimization objectives, with the letter symbol z as the design constant, and θp illustrating the estimated variance of the optimization design objectives. Nonetheless, the letter symbol S_{com} depicts the systematic and comprehensive design sensitivity coefficient, utilizing the synergy of the single sensitivity design coefficient for the average output torque, denoted as S_{Tavg} and the torque ripple presented as S_{Trip} in Equation (4).

Nonetheless, the low-sensitivity design parameters unveiled by both the designed Stator PMFS motor and the Spoke-Type IPM configured motor analysis exhibited an infinitesimal influence on the output torque of the optimization target. However, the single-parameter FEA methodology is employed or utilized to optimize the obtained low-sensitivity design parameters.

Moreover, the Bare-Bones Multi-Objective Particle Swarm Optimization (BB_MOPSO) design algorithm is adopted for high-sensitivity design parameter optimization and evaluation to unveil minimal output torque ripple and its corresponding maximum output torque in the two aforementioned motors, namely, the configured Stator PMFS motor model and the design Spoke-Type IPM motor model, which also includes a comprehensive analysis. Meanwhile, an extensive detail and analysis of the BB_MOPSO) technique or optimization process can be traced in [59, 60].

Furthermore, the average electromagnetic torque waveforms unveiled before and after the optimization of the Stator PMFS motor and Spoke-Type IPM configured motor designs are systematically illustrated in Figure 7(a) and (b), respectively. However, in analyzing the final design optimization based on the design objectives, the Stator PMFS motor exhibited an average electromagnetic torque of 6.46 Nm with a design torque ripple generation of 3.93%, while the Spoke-Type IPM motor unveiled an electromagnetic torque of 7.65 Nm with a corresponding torque ripple of 3.84%. Besides, it is essential to establish or highlight that the modeled Spoke-Type IPM motor exhibited an improved or enhanced output operating torque of 18.4% with an output torque ripple reduction of 2.3% compared to the Stator PMFS motor design.

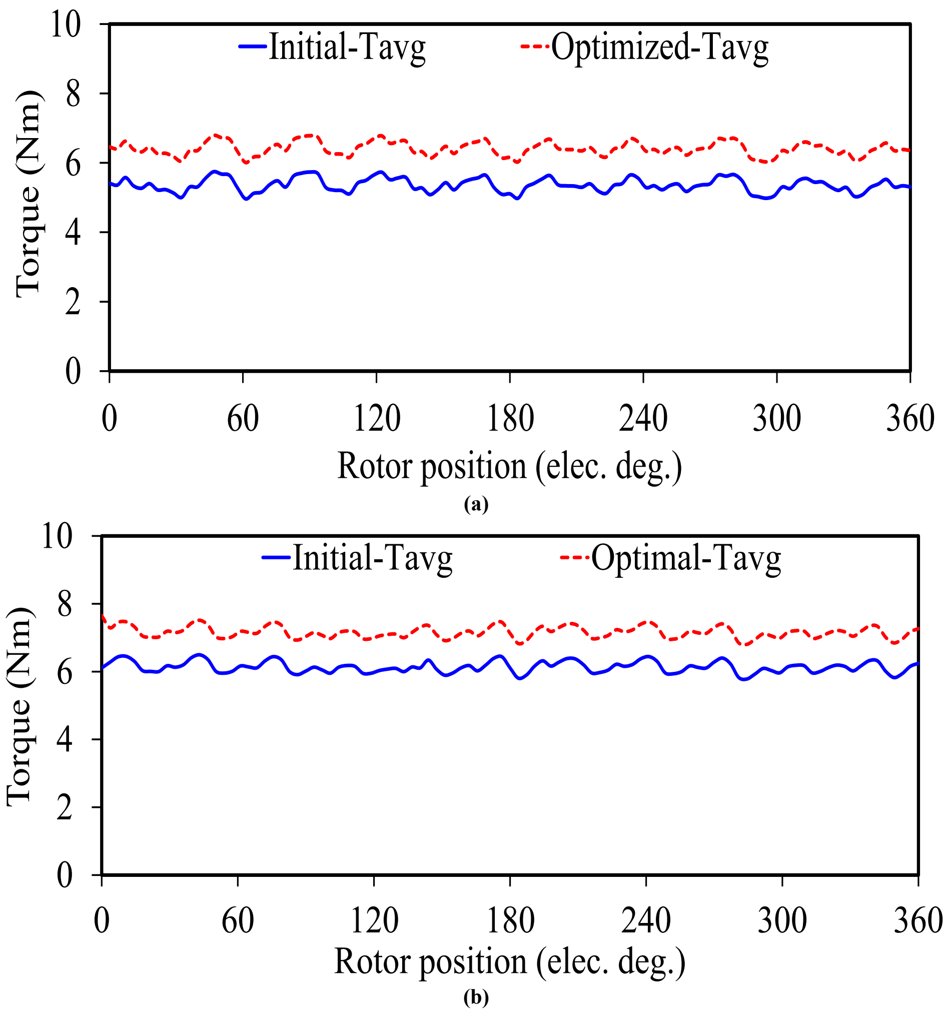

Fig. 7 Average torque analysis before and after optimization (a) Stator PMFS motor, and (b)Spoke-Type IPM motor.

4. Results and Discussion

4.1. Design No-Load Condition Analysis of Stator PMFS Motor and Spoke-Type IPM Motor

4.1.1. Performance Evaluation of Design Flux-Density and Airgap Flux-Density

The flux-density and the established flux-lines of the Stator PMFS motor and Spoke-Type IPM motor during the no-load operating conditions are presented or depicted in Figure 8 (a) and (b), respectively. Furthermore, to ensure intuitive design analysis, it is essential to highlight that the flux-density and the flux-lines of the Stator PMFS motor are presented in Figure 8 (a), while the flux-density and flux-lines or linkage of the Spoke-Type IPM motor are illustrated in Figure 3 (b). Also, it is important to point out that the flux-density and flux-linkage or flux-lines scales are shown in Figure 8 (c). Moreover, the flux lines established by both motors depicted in Figure 8 (a) and (b), respectively, are comparable. Nonetheless, based on the unveiled flux-density distribution analysis of the two design motors as shown in Figure 8 (b) and (b), it clearly depicts that the Stator PMFS motor unveils slightly higher overload operating capabilities, in that the Spoke-Type IPM motor unveils a slightly higher stator teeth and rotor rib saturation as illustrated in Figure 8 (b), when compared to the Stator PMFS motor in Figure 8 (a).

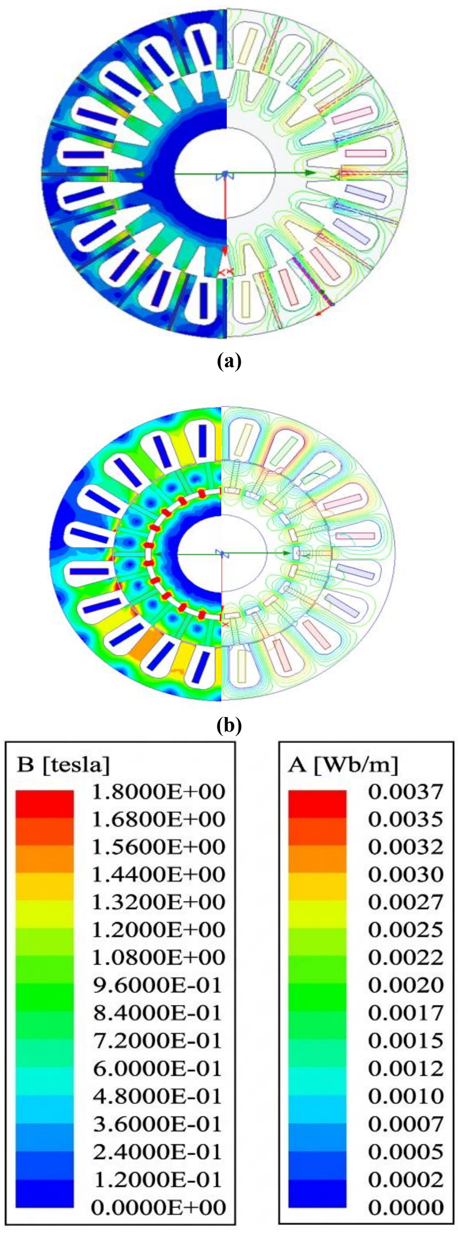

Fig. 8 Flux-Density analysis (a) Flux-Density and Flux-Linkage of the stator PMFS motor (b) Flux-Density and Flux-Linkage of Spoke-Type IPM motor, and (c) Flux-Density and Flux-linkage scales.

Moreover, the radial and tangential generated flux densities of the Stator PMFS motor and Spoke-Type IPM motor, which are key design components of a Permanent Magnet (PM) motor to ensure an enhanced electromagnetic torque, minimal torque ripple production with improved efficiency, etc., are presented or illustrated in Figures 9 (a) and (b), respectively. Meanwhile, it is essential to emphasize that the radial flux density unveiled by the spoke-type IPM-configured motor, as depicted in Figure 9 (a), is marginally higher than that of the Stator PMFS motor, resulting in slightly higher stator teeth (iron core) saturation in the Spoke-Type IPM-configured motor as illustrated in Figure 8 (b). Although an enhanced radial flux density is a good design signal, but too high a value will affect the motor overload capacity. Nonetheless, the Stator PMFS motor exhibits higher tangential flux density, which is key in torque contribution, compared to the Spoke-Type IPM motor as presented in Figure 9 (b). However, too high a tangential flux density can be a distraction to the motor. Hence, the two motors considered in this paper balanced the production of radial and tangential components of flux densities in a safe operating range and from a design point of view.

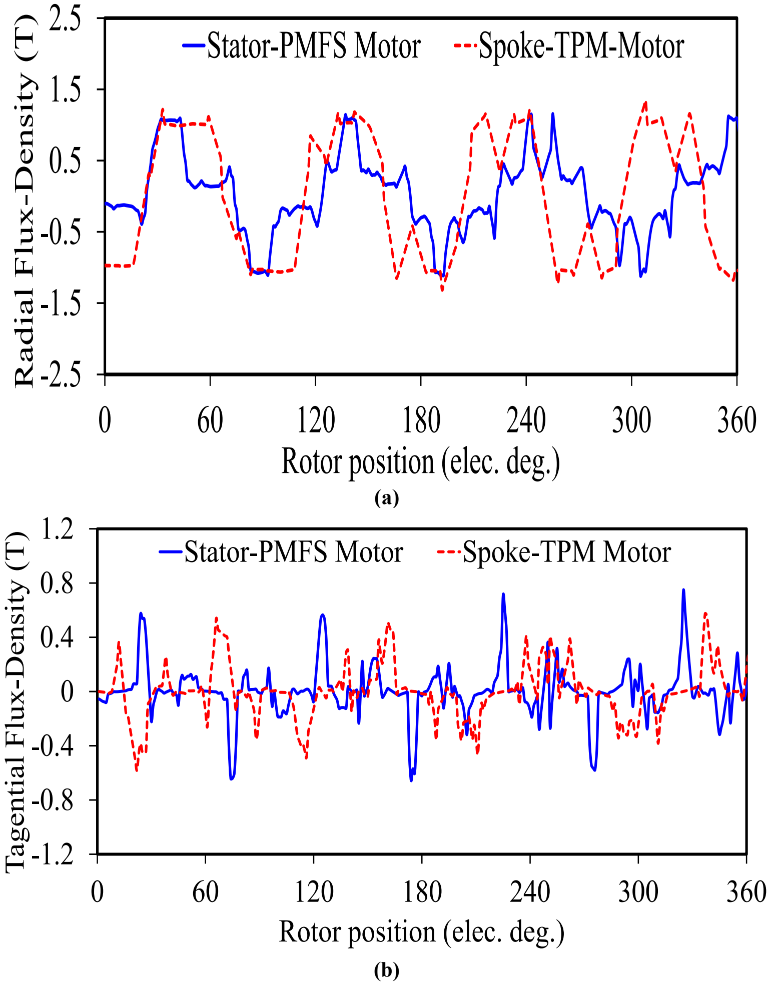

Fig. 9 Airgap Flux-density analysis (a) Radial Flux-Density, and (b) Tangential Flux-Density.

4.1.2. Performance Evaluation of No-Load Operating Back Electromotive Force of Stator PMFS Motor and Spoke-Type IPM Motor

The no-load derived produced Back Electromotive Force (Back-EMF) of the Stator PMFS motor and Spoke-Type IPM motor is presented in Figures 10 (a) and (b). Moreover, both motors exhibit sinusoidal waveforms, with the Spoke-Type IPM motor showing higher generated back-EMF and greater distortion than the designed Stator PMFS motor, as illustrated in Figure 10 (a). However, it is imperative to highlight that the higher back-EMF exhibition of the Spoke-Type IPM motor significantly influences the output electromagnetic torque. Nonetheless, it is equally important to indicate that the smooth sinusoidal waveform exhibition of the Stator PMFS motor guarantees a potentially smooth motor operation. Furthermore, the harmonic-order waveform of the back-EMF is illustrated or presented in Figure 10 (b). However, in multiphase motors, especially a five-phase motor, the 9th, 11th, 19th, and 21st harmonic orders are significant contributors or causes of torque ripples with an accompanying vibration and acoustic sound, which is higher in the designed Spoke-Type IPM motor compared to the Stator PMFS motor, as shown in Figure 10 (b).

Besides, the Total Harmonic Distortion (THD) unveiled by the Spoke-Type IPM configured motor is 18.43%, compared to the Stator PMFS motor of 1.69%. Meanwhile, it is essential to emphasize that the Stator PMFS motor exhibits 90.8% THD reduction compared to the Spoke-Type IPM configured motor.

Furthermore, the THD can be calculated via the formula given in Equation (5).

$$\mathrm{THD} = \frac{\sqrt{\sum_{z=2}^{\infty} E_z^2}}{E_1} = \frac{\sqrt{\left(E_2^2 + E_3^2 + E_3^2 + E_4^2 + E_5^2 + \ldots\right)}}{E_1} \times 100\% \qquad (5)$$

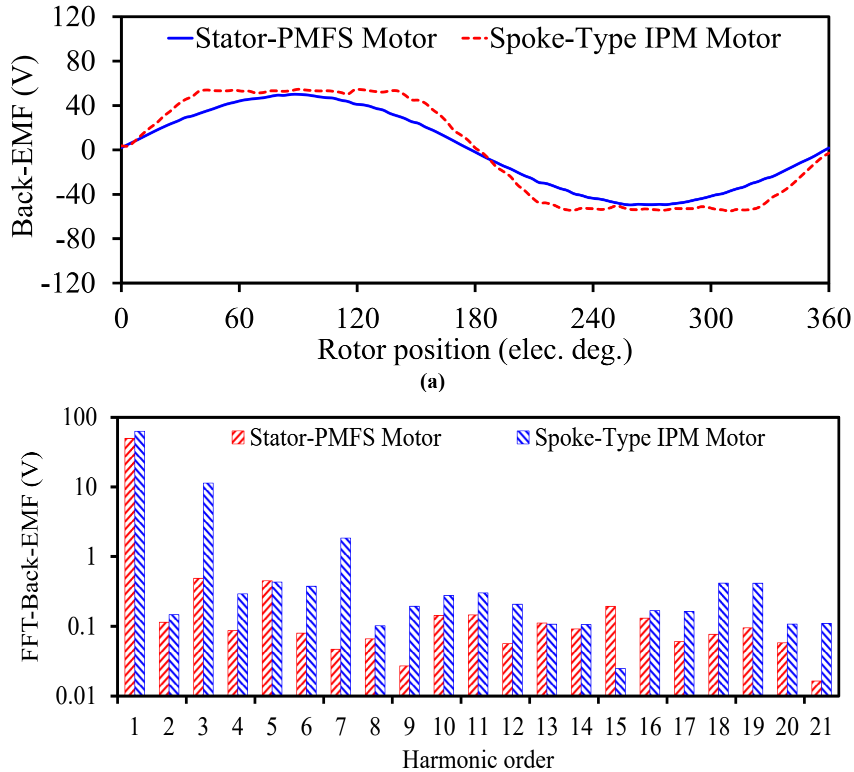

(a)

(b)

Fig. 10 Design analysis of the Back-EMF of the Stator PMFS motor and Spoke-Type IPM motor (a) Back-EMF waveform, and (b) Harmonic order waveform.

4.1.3. Analysis and Evaluation of the Torque Output Performance of the Stator PMFS Motor and Spoke-Type Motor

The design or motor cogging torque, which is defined as the torque ripple caused via the interactions between the configured Permanent Magnets (PMs) and the laminated stator slots or teeth, even though no current is injected into the windings of the motor, is analyzed in both the Stator PMFS motor and Spoke-Type IPM motor considered in this paper.

Nonetheless, the cogging torque performance analysis waveform of the Stator PMFS motor and Spoke-Type IPM motor is shown in Figure 11. Additionally, the Spoke-Type IPM motor exhibits a higher cogging torque than its Stator PMFS motor counterpart. Moreover, for intuitive analysis, the Spoke-Type IPM motor exhibited a torque of 0.43 Nm, while that of the Stator PMFS motor was 0.39 Nm. Hence, depicting a reduction of 0.4 Nm in the Stator PMFS motor compared to the Spoke-Type IPM motor. To ensure a significant and comprehensive reduction in the amplitude of cogging torque and to achieve a higher or enhanced number of periods (NT) exhibited in the obtained cogging torque waveforms, the same design slot pole synergy, that is, 20 stator slots and 11 rotor pole pairs, is selected for both the Stator PMFS motor and Spoke-Type IPM motor, and also to ensure fair design comparison. Moreover, the NT can be computed in Equation (6).

$$N_T = \frac{2p}{GCD\left(Q_s, 2p\right)} \qquad (6)$$

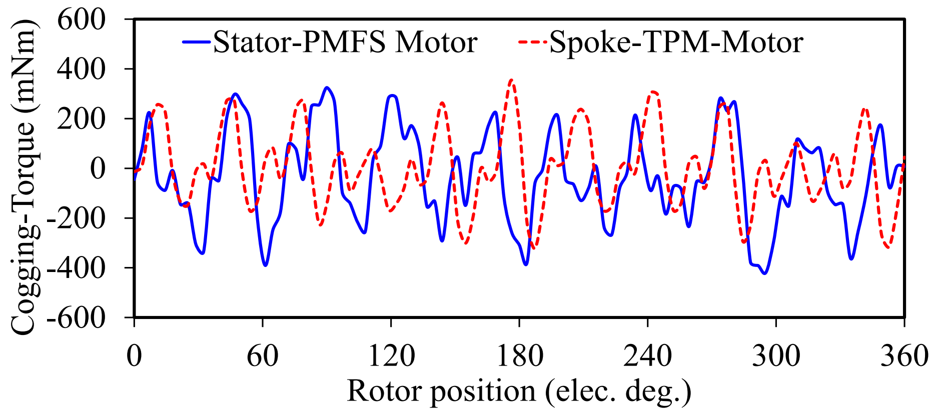

Fig. 11 Design cogging torque analysis of the Stator PMFS motor and Spoke-Type IPM motor

However, it is vital to emphasize that the Spoke-Type IPM motor unveiled a higher electromagnetic torque compared to the Stator PMFS motor, as presented in the torque waveform analysis in Figure 12. Nevertheless, for intuitive design performance analysis, the Spoke-Type IPM motor exhibited 7.65 Nm, while the Stator PMFS motor unveiled 6.46 Nm. Hence, indicating 18.42% increase in the Spoke-Type IPM motor compared to the Stator PMFS motor, as shown in Tables 2 and 3, also, buttress in Figure 12 (b).

Furthermore, the average electromagnetic torque at various current angles ranging from 0^0 to 50^o. Besides, it is essential to emphasize that the Spoke-Type IPM motor exhibits higher torque at various selected current angles compared to the Stator PMFS motor, as illustrated in Figure 12 (b). Meanwhile, it is essential to emphasize that the Spoke-Type IPM motor unveils minimal torque ripple at various selected or computed current angles compared to the Stator PMFS motor, as shown in Figure 12 (c). Nonetheless, the operating torque ripple can be computed in Equation (7).

$$T_{rip} = \frac{T_{pk-pk}}{T_{avg}} \times 100\% \tag{7}$$

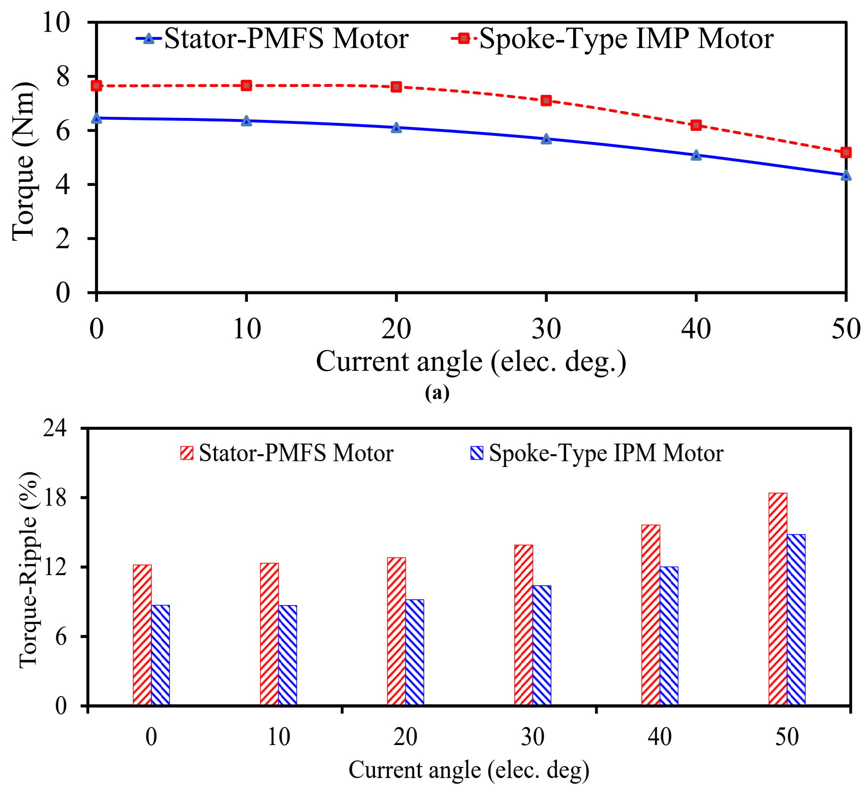

(a)

(b)

Fig. 12 Electromagnetic torque performance analysis (a) Average torque analysis at various current angles, and (b) Torque ripple analysis at various current angles.

4.1.4. Design Losses and Efficiency Analysis

An electric motor's operating efficiency is essential from researchers' and designers' points of view because it is one of the key design parameters for assessing performance and determining how efficient the motor is. Hence, to efficiently and systematically evaluate the operating performance of the Stator PMFS motor and Spoke-Type IPM motor, the design losses are chronologically presented in Figures 13(a), (b), and (c), respectively. Meanwhile, Figure 13(a) shows that the Spoke-Type IPM motor exhibited the highest stator losses among the motors. Nonetheless, it can equally be seen in Figures 13(b) and (c) respectively, that the Spoke-Type IPM motor exhibits the minimal rotor and PM losses compared to the Stator PMFS motor. Moreover, it is imperative to highlight that the aforementioned merits of loss reduction exhibited by the Spoke-Type IPM motor resulted in higher operating efficiency at all the various current angles compared to the Stator PMFS motor, as presented in Figure 13(d).

Besides, the efficiency exhibited by the Spoke-Type IPM motor at the current angle 0^0 is 93.24%, while that of the Stator PMFS motor is 92.16%, representing a 1.17% increase in the Spoke-Type IPM motor compared to the Stator PMFS motor. Moreover, the efficiency computation can be expressed in Equation (8). Furthermore, the rotational power of the motor can be derived from Equation (9)

$$\eta = \frac{P_{out}}{P_{in}} \times 100\% = \frac{T_{avg\omega m}}{T_{avg\omega m} + P_{CUL} + P_{PML} + P_{RTL} + P_{STL}} \times 100\% \tag{8}$$

$$P = \omega T = T\left(\frac{2\pi NT}{60}\right) = \frac{NT}{9.55} \tag{9}$$

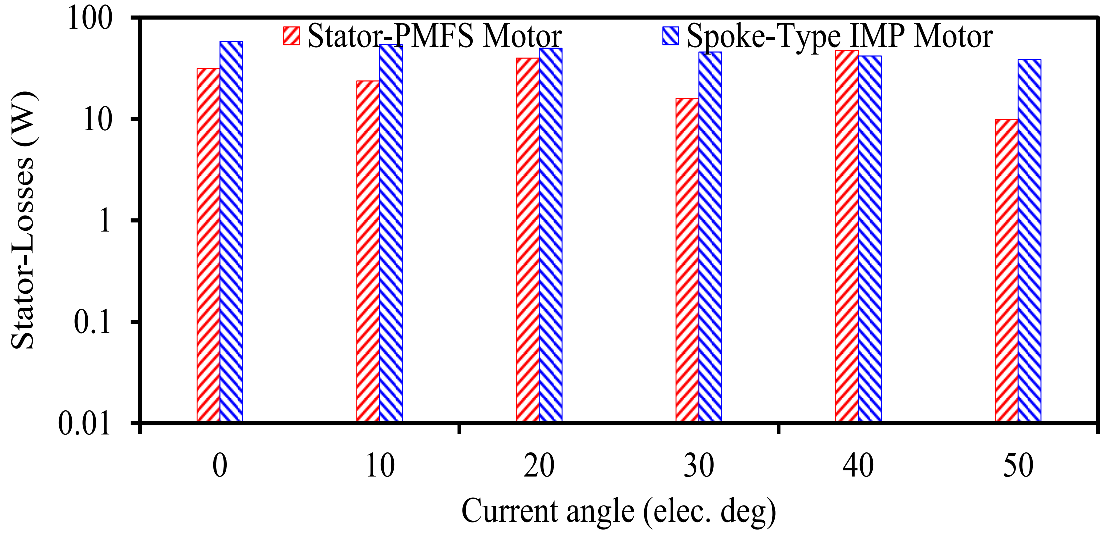

(a)

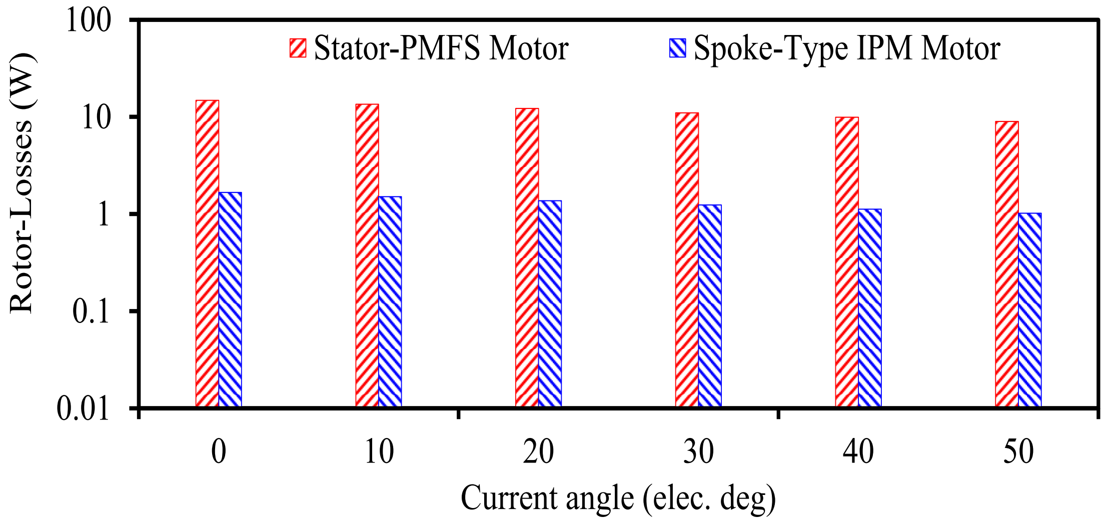

(b)

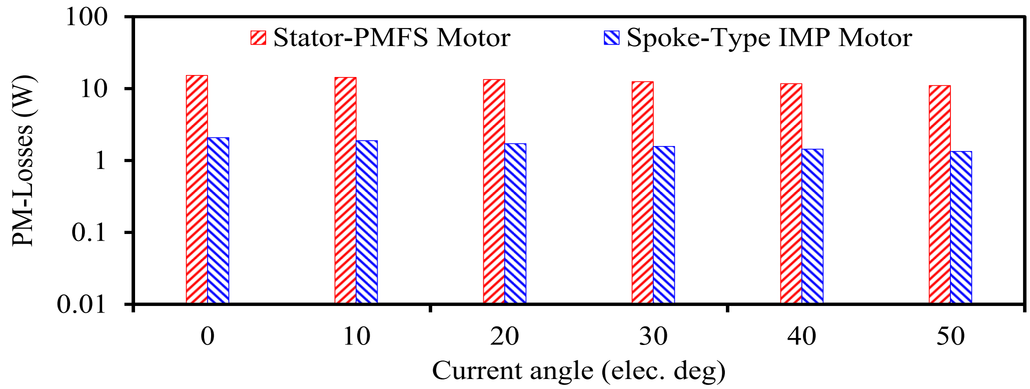

(c)

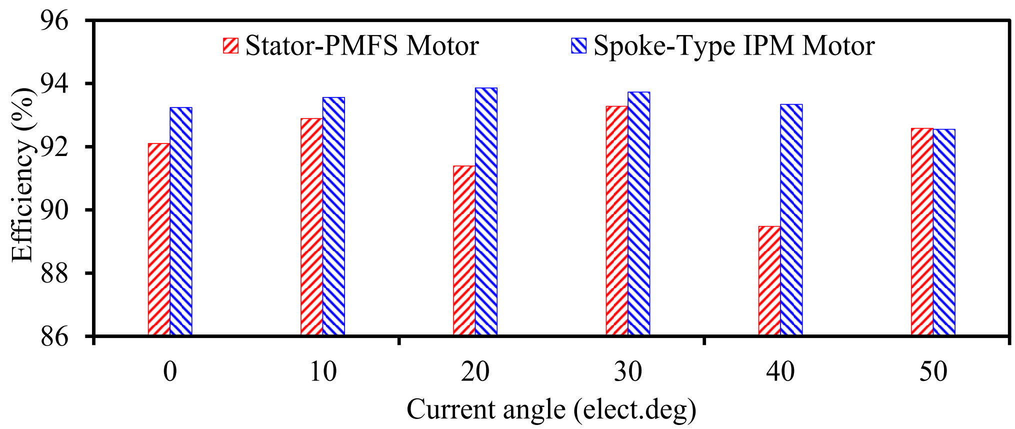

(d)

Fig. 13 Design losses and efficiency performance analysis (a) Stator design losses, (b) Rotor design losses, (c) PM design losses, and (d) Operating efficiency.

The power and torque densities of an electric motor are imperative for applications such as the traction of Electric Vehicles (EVs), aircraft, ships, drones, and robotics. Moreover, higher power density ensures reduction of weight, space saving, a smaller design motor for the same operating power, and high performance.

Nonetheless, higher torque density enables a higher starting torque from a compact motor size, which is key or useful in EVs traction and key in robotics. Hence, from an electric motor design analysis and research point of view, optimizing and improving or enhancing the power and torque densities are the primary aim of ensuring that the designed motors are smaller, lightweight, robust, and cost-effective or more efficient.

Therefore, the power density analysis and torque density analysis of the Stator PMFS motor and Spoke-Type IPM configured motor are effectively considered in this research paper. Moreover, the computed power density of the Stator PMFS motor and Spoke-Type IPM configured motor at the current angle $0^o$are 1.2 kW/L and 1.41 kW/L, respectively. Hence, exhibiting 17.5% increase in the Spoke-Type IPM configured motor compared to the Stator PMFS motor. Nevertheless, the torque density of the Stator PMFS motor is 7.6 Nm/L, while the Spoke-Type IPM motor unveiled 9 Nm/L. Hence, depicting an 18.42% increase in the Spoke-Type IPM motor compared to the Stator PMFS motor. To ensure an intuitive analysis, the obtained design parameter specifications are presented or illustrated in Table 6.

Table 6. Analysis and evaluation of operating power and torque densities between the stator PMFS motor and the Spoke-Type IPM motor at current angle 0°

Design Parameter Specification	Stator PMFS Motor	Spoke-Type IPM Motor
Average torque (Nm)	6.46	7.65
Output-Power (W)	1014.66	1201.57
Volume (L)	0.85	0.85
Power Density (kW/L)	1.2	1.41
Torque Density (Nm/L)	7.60	9.00

4.1.5. Magnetic Phase Isolation Analysis and Evaluation of Stator PMFS Motor and Spoke-Type IPM Motor

Self and mutual inductance analysis in electric motor design is a critical design consideration in that it ensures smooth and safe operation, especially in the event of a fault. Moreover, higher motor self-inductance assists in the reduction of sudden rises or changes in current, hence ensuring smooth motor operation. Thus, higher motor self-inductance can obviously limit the motor's short-circuit current. Nonetheless, a lower mutual inductance of a motor is suitable, especially in fault-tolerant motor designs, because it ensures that a fault detection or occurrence in one phase has less or no effect on another phase.

Hence, the self and mutual inductance of the five-phase fault-tolerant Stator PMFS motor and Spoke-Type IPM motor analysis is considered in this paper. Furthermore, the Stator PMFS motor exhibits higher self-inductance, which is beneficial and vital for limiting short-circuit or fault current compared to the Spoke-Type motor, as shown in Figures 14(a) and 12 (b), respectively. Nonetheless, imperative to highlight that the Spoke-Type IPM motor unveils a lower mutual inductance, which is beneficial in limiting phase interaction, as shown in Figure 14 (b) compared to the Stator PMFS motor in Figure 14(a).

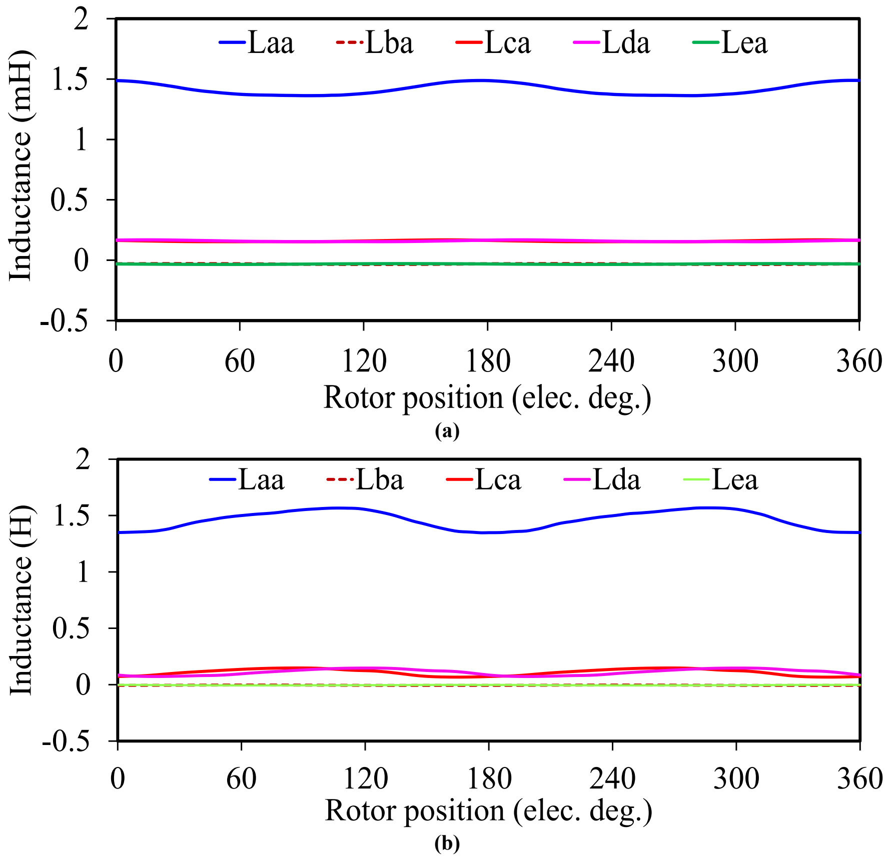

Fig. 14 Analysis and evaluation of Sel and mutual inductance (a) Stator PMFS motor, and (b) Spoke-Type IPM motor.

5. Conclusion

The design of the five-phase fault-tolerant Stator PMFS motor and Spoke-Type IMP motor with the same design parameters and specifications is extensively, systematically, and successfully compared in the research paper for Electric Vehicle (EV) traction applications via Finite Element Analysis (FEA). Moreover, the Spoke-Type IPM motor exhibits lower mutual inductance, thereby ensuring effective magnetic phase isolation so that, in the event of a fault on one phase, it does not adversely affect the other healthy phases, thereby ensuring a higher degree of freedom. Nonetheless, it is imperative to note that the Stator PMFS motor exhibits higher self-inductance, which is key to limiting short-circuit current compared to the Spoke-Type IPM motor. Furthermore, the Spoke-Type motor unveils a higher electromagnetic torque of 7.65 Nm with a corresponding higher operating efficiency of 93.24% compared to the Stator PMFS motor with an electromagnetic torque of 6.46 Nm with a corresponding efficiency of 92.16%. Meanwhile, the Stator PMFS motor exhibits a slightly minimal cogging torque compared to the Spoke-Type IPM motor, which is a positive impact. Besides, it is imperative to highlight that the Spoke-Type IPM motor unveils a minimal torque ripple compared to the Stator PMFS motor, which is key in EV traction applications. Also, the

Spoke-Type IPM motor exhibits a torque density of 9 Nm/L compared to the Stator PMFS motor of 7.6 Nm/L, respectively. Meanwhile, the power density obtained via the Spoke-Type IPM motor is 1.41 Kw/l, while that of the Stator PMFS motor is 1.2 Kw/L. From the aforementioned merits of the Spoke-Type IPM motor, it can firmly be concluded that the five-phase fault-tolerant Spoke-Type IPM motor is the preferred design candidate for EV traction applications compared to the five-phase fault-tolerant Stator PMFS motor design.

References

[1] Olaf Borsboom, Mauro Salazar, and Theo Hofman, "Electric Motor Design Optimization: A Convex Surrogate Modeling Approach," *IFAC-Papers Online*, vol. 55, no. 24, pp. 373-378, 2022. [CrossRef] [Google Scholar] [Publisher Link]

[2] C.C. Awah et al., "Comparison of Partitioned Stator Switched Flux Permanent Magnet Machines Having Single- or Double-Layer Windings," *IEEE Transactions on Magnetics*, vol. 52, no. 1, pp. 1-10, 2016. [CrossRef] [Google Scholar] [Publisher Link]

[3] S.E. Rauch, and L.J. Johnson, "Design Principles of Flux-switch Alternators [Includes Discussion]," *Transactions of the American Institute of Electrical Engineers. Part III: Power Apparatus and Systems*, vol. 74, no. 3, pp. 1261-1268, 1995. [CrossRef] [Google Scholar] [Publisher Link]

[4] Emmanuel Hoang, Hamid Ben Ahmed, and Jean Lucidarme, "Switching Flux Permanent Magnet Polyphased Synchronous Machines," *Switching Flux Permanent Magnet Polyphased Synchronous Machines*, Trondheim, Norway, 1997. [Google Scholar] [Publisher Link]

[5] Z.Q. Zhu et al., "Analysis of Electromagnetic Performance of Flux-switching Permanent-Magnet Machines by Nonlinear Adaptive Lumped Parameter Magnetic Circuit Model," *IEEE Transactions on Magnetics*, vol. 41, no. 11, pp. 4277-4287, 2005. [CrossRef] [Google Scholar] [Publisher Link]

[6] Emmanuel Hoang, Michel Lecrivain, and Mohamed Gabsi, "A New Structure of a Switching Flux Synchronous Polyphased Machine with Hybrid Excitation," *2007 European Conference on Power Electronics and Applications*, Aalborg, Denmark, pp. 1-8, 2007. [CrossRef] [Google Scholar] [Publisher Link]

[7] Wei Hua et al., "Analysis and Optimization of Back EMF Waveform of a Flux-Switching Permanent Magnet Motor," *2007 IEEE International Electric Machines and Drives Conference*, Antalya, Turkey, pp. 1025-1030, 2007. [CrossRef] [Google Scholar] [Publisher Link]

[8] J.T. Chen, and Z.Q. Zhu, "Comparison of All- and Alternate-Poles-Wound Flux-Switching PM Machines Having Different Stator and Rotor Pole Numbers," *IEEE Transactions on Industry Applications*, vol. 46, no. 4, pp. 1406-1415, 2010. [CrossRef] [Google Scholar] [Publisher Link]

[9] Richard L. Owen et al., "Alternate Poles Wound Flux-Switching Permanent-Magnet Brushless AC Machines," *IEEE Transactions on Industry Applications*, vol. 46, no. 2, pp. 790-797, 2010. [CrossRef] [Google Scholar] [Publisher Link]

[10] Z.Z. Wu, and ZQ. Zhu, "Analysis of Air-Gap Field Modulation and Magnetic Gearing Effects in Switched Flux Permanent Magnet Machines," *IEEE Transactions on Magnetics*, vol. 51, no. 5, pp. 1-12, 2015. [CrossRef] [Google Scholar] [Publisher Link]

[11] Tsarafidy Raminosoa, Chris Gerada, and Michael Galea, "Design Considerations for a Fault-Tolerant Flux-Switching Permanent-Magnet Machine," *IEEE Transactions on Industrial Electronics*, vol. 58, no. 7, pp. 2818-2825, 2011. [CrossRef] [Google Scholar] [Publisher Link]

[12] J.T. Chen, and Z.Q. Zhu, "Winding Configurations and Optimal Stator and Rotor Pole Combination of Flux-Switching PM Brushless AC Machines," *IEEE Transactions on Energy Conversion*, vol. 25, no. 2, pp. 293-302, 2010. [CrossRef] [Google Scholar] [Publisher Link]

[13] Lingyun Shao et al., "A Comparative Study on Nine- and Twelve-Phase Flux-Switching Permanent-Magnet Wind Power Generators," *IEEE Transactions on Industry Applications*, vol. 55, no. 4, pp. 3607-3616, 2019. [CrossRef] [Google Scholar] [Publisher Link]

[14] Emil Levi, "Multiphase Electric Machines for Variable-Speed Applications," *IEEE Transactions on Industrial Electronics*, vol. 55, no. 5, pp. 1893-1909, 2008. [CrossRef] [Google Scholar] [Publisher Link]

[15] Steve Williamson, Sandy Smith, and Chris Hodge, "Fault Tolerance in Multiphase Propulsion Motors," *Journal of Marine Engineering and Technology*, vol. 3, no. 1, pp. 3-7, 2004. [CrossRef] [Google Scholar] [Publisher Link]

[16] L. Parsa, "On Advantages of Multi-phase Machines," *31st Annual Conference of IEEE Industrial Electronics Society, 2005. IECON 2005*, Raleigh, NC, USA, 2005. [CrossRef] [Google Scholar] [Publisher Link]

[17] Stephane Brisset, Darius Vizireanu, and Pascal Brochet, "Design and Optimization of a Nine-Phase Axial-Flux PM Synchronous Generator with Concentrated Winding for Direct-Drive Wind Turbine," *IEEE Transactions on Industry Applications*, vol. 44, no. 3, pp. 707-715, 2008. [CrossRef] [Google Scholar] [Publisher Link]

[18] Emine Bostanci et al., "Opportunities and Challenges of Switched Reluctance Motor Drives for Electric Propulsion: A Comparative Study," *IEEE Transactions on Transportation Electrification*, vol. 3, no. 1, pp. 58-75, 2017. [CrossRef] [Google Scholar] [Publisher Link]

[19] Jiahong Zhuang et al., "Electromagnetic Performances Analysis of a Hybrid-Permanent-Magnet Motor Capable of High Torque," *2019 22nd International Conference on Electrical Machines and Systems (ICEMS)*, Harbin, China, pp. 1-4, 2019. [CrossRef] [Google Scholar] [Publisher Link]

[20] Salar Ahmad Khalil et al., "Design and Optimization of High Torque Density Spoke-type Inverted V Shape IPMSM with Concentrated Winding for EV Applications," *Results in Engineering*, vol. 26, pp. 1-13, 2025. [CrossRef] [Google Scholar] [Publisher Link]

[21] Jincheng Yu et al., "Comparative Study of Double-Stator Interior-PM Vernier Machines based on Electromagnetic-Structural Coupling Analysis," *IEEE Transactions on Industrial Electronics*, vol. 68, no. 11, pp. 10510-10520, 2021. [CrossRef] [Google Scholar] [Publisher Link]

[22] Yang Xiao et al., "Influence of Armature Reaction on Magnetic-Field-Shifting Effect in Asymmetric Interior Permanent Magnet Machines," *IEEE Transactions on Energy Conversion*, vol. 37, no. 2, pp. 1475-1488, 2022. [CrossRef] [Google Scholar] [Publisher Link]

[23] Gerd Bramerdorfer et al., "More Robust and Reliable Optimized Energy Conversion Facilitated through Electric Machines, Power Electronics and Drives, and Their Control: State-of-the-Art and Trends," *IEEE Transactions on Energy Conversion*, vol. 35, no. 4, pp. 1997-2012, 2020. [CrossRef] [Google Scholar] [Publisher Link]

[24] Kang Ma et al., "Design Optimization of a Spoke-Type Permanent Magnet Motor for Torque Performance Improvement," *IEEE Transactions on Energy Conversion*, vol. 41, no. 2, pp. 1004-1016, 2026. [CrossRef] [Google Scholar] [Publisher Link]

[25] Qian Chen et al., "Design and Optimization of a New Spoke-Type Flux-Modulation Machine with Inverted T-Shape Permanent Magnets," *IEEE Transactions on Energy Conversion*, vol. 38, no. 1, pp. 203-217, 2023. [CrossRef] [Google Scholar] [Publisher Link]

[26] Yang Xiao et al., "A Novel Spoke-Type Asymmetric Rotor Interior Permanent Magnet Machine," *IEEE Transactions on Industry Applications*, vol. 57, no. 5, pp. 4840-4851, 2021. [CrossRef] [Google Scholar] [Publisher Link]

[27] Dawei Li et al., "Analysis of Fractional-Slot Concentrated Winding PM Vernier Machines with Regular Open-Slot Stators," *IEEE Transactions on Industry Applications*, vol. 54, no. 2, pp. 1320-1330, 2018. [CrossRef] [Google Scholar] [Publisher Link]

[28] Cheng Gong, and Fang Deng, "Design and Optimization of a High-Torque-Density Low-Torque-Ripple Vernier Machine using Ferrite Magnets for Direct-Drive Applications," *IEEE Transactions on Industrial Electronics*, vol. 69, no. 6, pp. 5421-5431, 2022. [CrossRef] [Google Scholar] [Publisher Link]

[29] Xiao Ge et al., "A Spoke-Type IPM Machine with Novel Alternate Airspace Barriers and Reduction of Unipolar Leakage Flux by Step-Staggered Rotor," *IEEE Transactions on Industry Applications*, vol. 52, no. 6, pp. 4789-4797, 2016. [CrossRef] [Google Scholar] [Publisher Link]

[30] Wenliang Zhao, Thomas A. Lipo, and Byung-II Kwon, "Torque Pulsation Minimization in Spoke-type Interior Permanent Magnet Motors with Skewing and Sinusoidal Permanent Magnet Configurations," *IEEE Transactions on Magnetics*, vol. 51, no. 11, pp. 1-4, 2015. [CrossRef] [Google Scholar] [Publisher Link]

[31] Qian Chen et al., "A Novel Spoke-Type PM Motor with Auxiliary Salient Poles for Low Torque Pulsation," *IEEE Transactions on Industrial Electronics*, vol. 67, no. 6, pp. 4762-4773, 2020. [CrossRef] [Google Scholar] [Publisher Link]

[32] Xiang Ren et al., "Analysis of Spoke-Type Brushless Dual-Electrical-Port Dual-Mechanical-Port Machine with Decoupled Windings," *IEEE Transactions on Industrial Electronics*, vol. 66, no. 8, pp. 6128-6140, 2019. [CrossRef] [Google Scholar] [Publisher Link]

[33] Jiaxuan Huang et al., "Design Method and Performance Evaluation of Modular Multiphase PMSM with Hybrid Single/Double Layer Fractional-Slot Concentrated Winding," *Journal of Electrical Engineering and Technology*, vol. 17, no. 5, pp. 2737-2751, 2022. [CrossRef] [Google Scholar] [Publisher Link]

[34] Sung-II Kim et al., "Investigation and Experimental Verification of a Novel Spoke-Type Ferrite-Magnet Motor for Electric-Vehicle Traction Drive Applications," *IEEE Transactions on Industrial Electronics*, vol. 61, no. 10, pp. 5763-5770, 2014. [CrossRef] [Google Scholar] [Publisher Link]

[35] Alireza Fatemi et al., "Design Optimization of a High Torque Density Spoke-Type PM Motor for a Formula E Race Drive Cycle," *IEEE Transactions on Industry Applications*, vol. 54, no. 5, pp. 4343-4354, 2018. [CrossRef] [Google Scholar] [Publisher Link]

[36] Xiaohong Xue et al., "Design of Five-Phase Modular Flux-Switching Permanent-Magnet Machines for High Reliability Applications," *IEEE Transactions on Magnetics*, vol. 49, no. 7, pp. 3941-3944, 2013. [CrossRef] [Google Scholar] [Publisher Link]

[37] David G. Dorrell, Min-Fu Hsieh, and Andrew M. Knight, "Alternative Rotor Designs for High Performance Brushless Permanent Magnet Machines for Hybrid Electric Vehicles," *IEEE Transactions on Magnetics*, vol. 48, no. 2, pp. 835-838, 2012. [CrossRef] [Google Scholar] [Publisher Link]

[38] Wenping Cao et al., "Overview of Electric Motor Technologies used for More Electric Aircraft (MEA)," *IEEE Transactions on Industrial Electronics*, vol. 59, no. 9, pp. 3523-3531, 2012. [CrossRef] [Google Scholar] [Publisher Link]

[39] Martin D. Hennen et al., "Development and Control of an Integrated and Distributed Inverter for a Fault Tolerant Five-Phase Switched Reluctance Traction Drive," *IEEE Transactions on Power Electronics*, vol. 27, no. 2, pp. 547-554, 2012. [CrossRef] [Google Scholar] [Publisher Link]

[40] A.M. El-Refaie, "Fault-tolerant Permanent Magnet Machines: A Review," *IET Electric Power Applications*, vol. 5, no. 1, pp. 59-74, 2011. [CrossRef] [Google Scholar] [Publisher Link]

[41] Ming Cheng et al., "Overview of Stator-Permanent Magnet Brushless Machines," *IEEE Transactions on Industrial Electronics*, vol. 58, no. 11, pp. 5087-5101, 2011. [CrossRef] [Google Scholar] [Publisher Link]

[42] Li Zhang et al., "Multiple Operation Design and Optimization of a Five-Phase Interior Permanent Magnet Motor Considering Compound Fault Tolerance from Perspective of Flux-Intensifying Effect," *IEEE Transactions on Transportation Electrification*, vol. 10, no. 4, pp. 9043-9054, 2024. [CrossRef] [Google Scholar] [Publisher Link]
[43] Adrian Baltatanu, and Marin-Leonard Florea, "Multiphase Machines used in Electric Vehicles Propulsion," *Proceedings of the International Conference on Electronics, Computers and Artificial Intelligence - ECAI-2013*, Pitesti, Romania, pp. 1-6, 2013. [CrossRef] [Google Scholar] [Publisher Link]
[44] Mohamed Y. Metwly et al., "Multiphase Stator Winding: New Perspectives, Advanced Topologies, and Futuristic Applications," *IEEE Access*, vol. 10, pp. 103241-103263, 2022. [CrossRef] [Google Scholar] [Publisher Link]
[45] Federico Barrero, and Mario J. Duran, "Recent Advances in the Design, Modeling, and Control of Multiphase Machines—Part I," *IEEE Transactions on Industrial Electronics*, vol. 63, no. 1, pp. 449-458, 2016. [CrossRef] [Google Scholar] [Publisher Link]
[46] E. Levi et al., "Multiphase Induction Motor Drives - A Technology Status Review," *IET Electric Power Applications*, vol. 1, no. 4, pp. 489-516, 2007. [CrossRef] [Google Scholar] [Publisher Link]
[47] Ruiwu Cao, Chris Mi, and Ming Cheng, "Quantitative Comparison of Flux-Switching Permanent-Magnet Motors with Interior Permanent Magnet Motor for EV, HEV, and PHEV Applications," *IEEE Transactions on Magnetics*, vol. 48, no. 8, pp. 2374-2384, 2012. [CrossRef] [Google Scholar] [Publisher Link]
[48] Amin Nobahari, Mehdi Aliahmadi, and Jawad Faiz, "Performance Modifications and Design Aspects of Rotating Flux Switching Permanent Magnet Machines: A Review," *IET Electric Power Applications*, vol. 14, no. 1, pp. 1-15, 2020. [CrossRef] [Google Scholar] [Publisher Link]
[49] Wenxiang Zhao et al., "Design and Analysis of a Linear Permanent- Magnet Vernier Machine with Improved Force Density," *IEEE Transactions on Industrial Electronics*, vol. 63, no. 4, pp. 2072-2082, 2016. [CrossRef] [Google Scholar] [Publisher Link]
[50] Dawei Li et al., "Synthesis of Flux Switching Permanent Magnet Machines," *IEEE Transactions on Energy Conversion*, vol. 31, no. 1, pp. 106-117, 2016. [CrossRef] [Google Scholar] [Publisher Link]
[51] Wenxiang Zhao et al., "Remedial Brushless AC Operation of Fault-Tolerant Doubly Salient Permanent-Magnet Motor Drives," *IEEE Transactions on Industrial Electronics*, vol. 57, no. 6, pp. 2134-2141, 2010. [CrossRef] [Google Scholar] [Publisher Link]
[52] Wenxiang Zhao et al., "Remedial Injected-Harmonic-Current Operation of Redundant Flux-Switching Permanent-Magnet Motor Drives," *IEEE Transactions on Industrial Electronics*, vol. 60, no. 1, pp. 151-159, 2013. [CrossRef] [Google Scholar] [Publisher Link]
[53] Guohai Liu et al., "Design and Analysis of a New Fault-Tolerant Permanent-Magnet Vernier Machine for Electric Vehicles," *IEEE Transactions on Magnetics*, vol. 48, no. 11, pp. 4176-4179, 2012. [CrossRef] [Google Scholar] [Publisher Link]
[54] Peng Su et al., "Analysis of the Operation Principle for Rotor-Permanent-Magnet Flux-Switching Machines," *IEEE Transactions on Industrial Electronics*, vol. 65, no. 2, pp. 1062-1073, 2018. [CrossRef] [Google Scholar] [Publisher Link]
[55] Enrico Carraro et al., "Design and Performance Comparison of Fractional Slot Concentrated Winding Spoke Type Synchronous Motors with Different Slot-Pole Combinations," *IEEE Transactions on Industry Applications*, vol. 54, no. 3, pp. 2276-2284, 2018. [CrossRef] [Google Scholar] [Publisher Link]
[56] Qian Chen et al., "Design of a Spoke-Type Permanent-Magnet Motor with Optimal Winding Configuration for Electric Vehicle Applications," *Journal of Applied Physics*, vol. 111, no. 7, 2012. [CrossRef] [Google Scholar] [Publisher Link]
[57] Wenliang Zhao, Thomas A. Lipo, and Byung-Il Kwon, "Dual-Stator Two-Phase Permanent Magnet Machines with Phase-Group Concentrated-Coil Windings for Torque Enhancement," *IEEE Transactions on Magnetics*, vol. 51, no. 11, pp. 1-4, 2015. [CrossRef] [Google Scholar] [Publisher Link]
[58] Kyu-Yun Hwang et al., "Rotor Pole Design in Spoke-Type Brushless DC Motor by Response Surface Method," *IEEE Transactions on Magnetics*, vol. 43, no. 4, pp. 1833-1836, 2007. [CrossRef] [Google Scholar] [Publisher Link]
[59] Xiaoyong Zhu et al., "Design and Optimization of a Flux-Modulated Permanent Magnet Motor based on an Airgap-Harmonic-Orientated Design Methodology," *IEEE Transactions on Industrial Electronics*, vol. 67, no. 7, pp. 5337-5348, 2020. [CrossRef] [Google Scholar] [Publisher Link]
[60] Guohai Liu et al., "Multiobjective Deterministic and Robust Optimization Design of a New Spoke-Type Permanent Magnet Machine for the Improvement of Torque Performance," *IEEE Transactions on Industrial Electronics*, vol. 67, no. 12, pp. 10202-10212, 2020. [CrossRef] [Google Scholar] [Publisher Link]